Hertzsprung gap stars as stellar merger progenitors

Author: Gerard Garia Moreno
Facultat de Física, Universitat de Barcelona, Diagonal 645, 08028 Barcelona, Spain.

Advisor: Nadejda Blagorodnova Mujortova
(Dated: June 15, 2023)

Abstract: Most close binary stars likely end their evolution in a merger, visible as a bright outburst named Luminous Red Nova (LRN). In this work, we investigated a sample of stars in the Milky Way aiming to find possible LRN progenitor binary systems based on their location in the HR diagram, their variability, their hydrogen emission, and their mid-infrared (mid-IR) excess. For a sample of 449017 stars with a luminosity and a color consistent with known LRN progenitors, we found that 3.7% (16731) are variable, 22% (97972) show emission on Hα or Hβ, and $\sim$0.5% ($\sim$2250) have mid-IR excess detected by the NEOWISE infrared space telescope. The lightcurves for a small set of $\sim$100 sources with variability, emission, and mid-IR excess suggest that new unstudied causes for their variability are present, which deserves further study.

I. INTRODUCTION

Luminous red novae (LRNe) are relatively new astrophysical transients. These kinds of outbursts have peak luminosities between that of classical novae and supernovae and are considered to be caused by the partial ejection of the common envelope (CE) that precedes the merging of binary stars [4]. The CE is a short-lived phase in the evolution of stellar binary systems. It forms when the primary star evolves in radius and fills its Roche lobe, starting mass-transfer to the secondary star [10]. Inside the CE, the stars spiral towards each other rapidly, decreasing their separation due to the transfer of angular momentum to the CE, which at some point might be fully or partially ejected. The outcome of this process is either a more compact binary or a fully merged star, respectively.

The most remarkable example of an LRN is *V1309 Scorpii* [14], caused by a merger of a contact binary. The system presented an interesting archival short-term variability that was interpreted as an eclipsing binary system. The outburst, detected in 2008, showed a rapid evolution—from an F-type giant to a K- and early M-type star on a scale of months—with an amplitude of 7–10 mag. After maximum brightness, the temperature of the photosphere decreased due to the progressive cooling of the ejected gas. Most known LRN progenitors are yellow giants (YG) or yellow supergiants (YSG). These stars are evolving off the main sequence (MS) and crossing the Hertzsprung gap (HG) towards the red giant branch (RGB). This phase is characterized by a rapid increase in the stellar radius. Because the presence of a nearby companion can initiate an unstable mass transfer, LRNe progenitors are stars in this region of the Hertzsprung-Russel (HR) diagram, which also present peculiar variability due to the mass transfer. Those LRNe with enough pre-outburst data showed a progressive brightening which is associated with gas escaping from the system and creating a larger pseudo-photosphere.

Based on the observational appearance of known LRN progenitors, a recent study [1] presented a method for identifying Galactic LRNe candidates likely to outburst within the next 1–10 years. The selection of candidates was based on the position in the HR diagram and the variability of the sources. From approximately 9.7×10^6 sources obtained from the *Gaia* Data Release 2 (DR2) and Early Data Release 3 (EDR3), 21 LRNe precursor candidates were selected that shared similar characteristics: the presence of Hα and (sometimes) Hβ emission lines together with the existence of an IR excess.

The new *Gaia* Data Release 3 (DR3) [9] provides calibrated spectra for 220 million sources out of 1800 million sources in the catalog. These spectra come from two photometers—the blue photometer (BP) and the red photometer (RP)—that cover the wavelength range 330-680 nm and 640-1050 nm, respectively [7]. A comparison of these spectra with the low-resolution spectra from *SPRAT* [12] (an instrument mounted on the Liverpool Telescope) spectroscopy is shown for one of the 21 LRNe precursors in Figure 1.

Taking advantage of the discovery potential of *Gaia* DR3 spectra, this paper offers a complementary approach to that of [1] and aims to further investigate the properties of stellar objects that are likely to be progenitors of LRNe. In this direction, an analysis of the emission, IR excess, and variability of a sample of stars in the HG was conducted. Once identified, LRNe progenitors can be observed before, during, and after the outburst takes place to enhance our knowledge of these kinds of transients and their progenitor systems.

II. METHODOLOGY

This section introduces the steps taken to determine the initial sample of sources and the analysis of their hydrogen line emission, variability, and IR excess. The photometric data for our analysis were obtained from the *Gaia* DR3 catalog and the mid-infrared catalog *ALLWISE* [6]. Extinction-corrected absolute magnitudes in the G band and the de-reddened BP-RP color were ob-

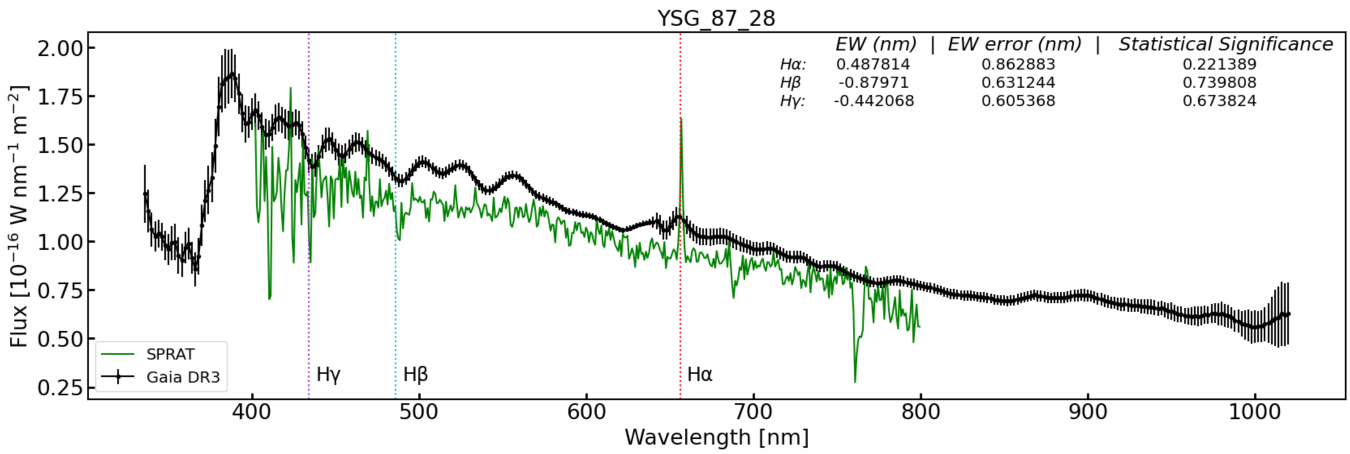

FIG. 1: Spectrum for the source YSG_87_28, one of the LRNe precursor candidates found in [1]. The black line shows the *Gaia* BP/RP spectrum from the DR3 and the green line the low-resolution spectrum from the *SPRAT* spectrograph. The main Balmer lines are identified. The top right table shows line strength expressed as equivalent width (EW), its error, and the statistical significance of the Balmer lines in the *Gaia* DR3 spectrum. Positive values of EW indicate emission and negative values indicate absorption.

tained from the *Gaia* EDR3 contribution *Starhorse* [2], which offered a more accurate extinction calculation. Stellar evolution tracks were obtained from the *MESA Isochrones & Stellar Tracks* [11] for stars in between 0.5 and 20 solar masses, with solar metallicity and initial rotation velocity of 40% the critical velocity. The spectroscopic data were obtained from the BP/RP spectra provided by *Gaia* DR3, accessible with the `Python` package `GaiaXPy`[1] [13]. It represents internally-calibrated mean spectra (with fluxes expressed in $e^{-}s^{-1}$), and spectra with physical units ($Wm^{-2}nm^{-1}$) covering the entire wavelength range covered by BP and RP.

A. Initial selection using the Color-Magnitud Diagram

The aim of our study is to examine the properties of stars in the HG, located between the MS and the RGB. Therefore, we selected a sample of stars based on their position on the CMD. Since our analysis focuses on evolving stars, we imposed a cut on the absolute magnitude $M_G < 1.5$, as stars above this magnitude have masses under $\sim$1.5M$_\odot$ and a 1.5M$_\odot$ becomes an RG in $\sim$20% the age of the Milky Way. To select sources between the MS and the RGB, we imposed two cuts with equations $(BP - RP) = (21/128)M_G + 149/386$ and $(BP - RP) = (-7/124)M_G + 603/620$. Lastly, we removed a portion of the CMD populated by Red Clump stars, known RGs in the horizontal branch. Our final sample is shown in Figure 2.

[1] https://gaia-dpci.github.io/GaiaXPy-website/

B. Line analysis

The study of emission for the strongest Balmer lines (Hα and Hβ) was conducted in collaboration with M. Weiler [15]. For our sample of HG stars, Weiler provided the equivalent width of the line, its error, and the statistical significance of the line in the internally calibrated spectrum. The table on the top right of Figure 1 shows an example of these data. The Hα emission is seen in both the BP/RP and the *SPRAT* spectrum. However, for the BP/RP spectrum, the error in the flux is large, which decreases its statistical significance. This can be explained by the possible variability of the source, which might show emission or absorption at different times. In order to include sources with variable emission in our analysis, we chose not to filter sources based on their error or their significance.

C. Variability study

Long- and short-term variability has been consistently detected for LRNe precursors. This variability can be linked to binary stars through eclipses or phenomena associated with the close contact between the two stars (mass transfer or pulsations, for example). The latter can lead to emission lines in the spectrum. Hence, we investigated the connection between variability and emission lines for our sample of HG stars.

We searched for variability using the *Gaia* DR3 flags `phot_variable_flag`, which indicates if variability was identified in the photometric data, and `vari_classifier_result`, which gives a classification for variable stars of different types. A table with the different types of variable stars can be found in the Appendix VI B.

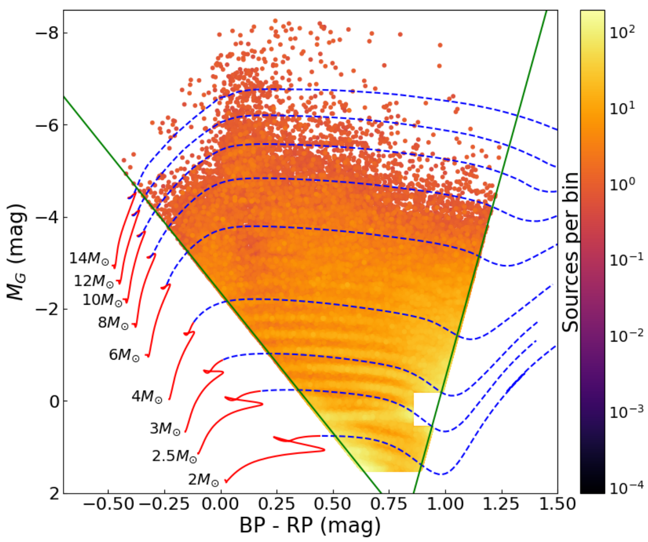

FIG. 2: Color-Magnitude Diagram showing the *Gaia* absolute magnitude in the G band (M_G) and BP-RP color for the stars in our sample selected (see Section II A). Both lines used to perform the cuts and the stellar evolutionary tracks for stars in the range of 2–14 solar masses are presented (the solid line corresponds to the main sequence).

To investigate if the emission was related to a particular type of variability, we inspected the Hα/Hβ emission strength for the different classes of variable stars present in the *Gaia* DR3 by analyzing their average spectrum. For each type, we compared the Hα emitters, the Hβ emitters, and all the stars (Figure 6, Appendix VI B).

Because the variability analysis in the *Gaia* catalog is incomplete, we also inspected the distribution of uncertainty on the G magnitude as a function of the same G (Figure 4) for all our sample and for sources classified as variables in the *Gaia* catalog (top), and for the sources with Hα or Hβ emission (bottom).

D. Study of mid-Infrared excess

The majority of LRN progenitors selected by [1] also showed a mid-IR excess in their spectral distribution, i.e. a greater measured mid-IR flux than expected. This extra flux can be associated with the presence of warm dust in an accretion disk or a cold envelope surrounding the source. To investigate the presence of this excess for our sample of Hα and Hβ emitters, we performed a cross-match with the *ALLWISE* catalog [6]. The *ALLWISE* catalog contains fluxes for 4 bandpasses: W1 (3.4 μm), W2 (4.6 μm), W3 (12 μm), and W4 (22 μm). To curate the IR data, quality cuts to the *ALLWISE* photometry were applied using the following flags: `cc_flags`, `ext_flag`, and `ph_qual` (see Appendix VI A). This ensured that the IR photometry had no nearby contamination and signal-to-noise ratio $S/N > 2$ in all 3 bands.

For the high-quality data sources, we compared the ones with Hα or Hβ emission with the ones without emission in a mid-IR Color-Color Diagram (CCD) (see Figure 5).

E. Light curves

We selected a group of sources that had all the expected characteristics for being LRN precursors: hydrogen emission, variability, and mid-IR excess. We removed the sources with known variability types in *SIMBAD* [16], and inspected the remaining light curves from the Zwicky Transient Facility (ZTF) [3] survey to find the possible origin for their variability. These light curves are shown in the Appendix VI C.

III. RESULTS

A. Emission and Variable stars

We compared the Hα/Hβ emission of stars identified and not identified as variables in *Gaia* to see if emission was associated with a certain type of variable star. From our initial sample of HG stars (449017), 22% (97972) presented Hα/Hβ emission. However, for the subgroup

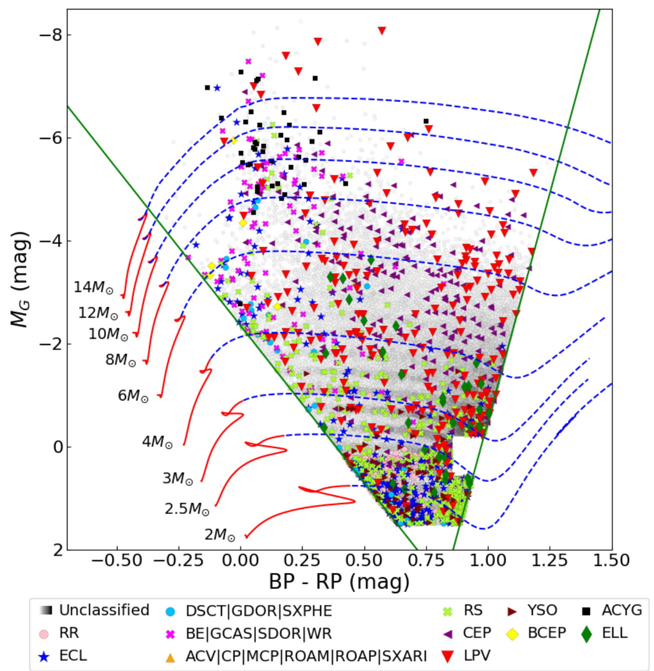

FIG. 3: Hα/Hβ emitter in our HG parameter space. Markers show different variability types from *Gaia* DR3 (see Appendix VI B). The stellar evolutionary tracks from *MESA* are included for information.

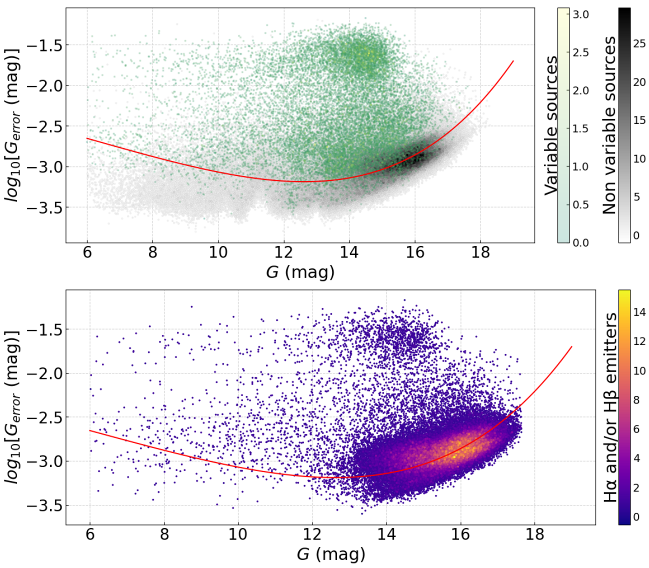

FIG. 4: *Gaia* G magnitude error as a function of the same G magnitude. Top: sources from our sample identified as variables and not variables in *Gaia*. Bottom: sources from our sample that show $H\alpha$ or $H\beta$ emission. The red curve in both graphs is a 5th-degree polynomial fitting the non-variable sources. Color bars show the number of sources per bin.

marked as variable in *Gaia*, 16% (2453) showed emission. In Figure 3 we see the emitters of different variable types and the emitters not identified as variable in our parameter space, both spread the same way.

To investigate if the *Gaia* identification of variable stars was incomplete, we inspected the G magnitude error of the sources on our sample. This is represented in Figure 4. The top part shows that the error in the magnitudes is related to the variability of the sources, as the distribution of error for variable stars is mostly above the average one for non-variable stars. The bottom part shows that even tho there is a significant amount of sources that could be (or already are) identified as variables, the majority of emitters in our whole sample are placed near the line related to expected errors. Thus, the presence of emission can be found in both variable and non-variable sources.

The inspection of average spectra for Hα and Hβ lines for each variable type revealed emission lines for a portion of stars in each variability type (see Appendix VI B).

B. Mid-IR excess for emitters and non-emitters

After applying the quality cuts to the *ALLWISE* data mentioned in Section II D, we were left with 4596 stars with IR data. From this IR bright sample of HG stars, 56% (2586) stars had Hα or Hβ emission and 44% (2010) had neither Hα nor Hβ. These stars are represented in a CCD with colors W1-W2 and W1-W4 (see Figure 5).

Both distributions for emitters and non-emitters are centered between the -0.1 and the 0 values in the W1-W2 axis, with some minor dispersion to both positive and negative values, a little bit more noticeable for emitters. On the W1-W4 axis, on the other hand, the distribution for non-emitters is centered around 0 with a tail expanding to positive values, and emitters show a distribution with more positive values.

IV. DISCUSSION

Emission lines among known variables are not unexpected. In our sample of HG stars, 10/11 subgroups of variable types are likely to show emission [8]: RR Lyrae variables show predominantly Hβ emission when they rise in brightness, in agreement with our findings; eruptive, hot, massive stars like Be stars, Gamma Cassiopeiae, S Doradus, Wolf-Rayet, and Alpha Cygni variables also display emission, which is often linked to accretion processes in their disks; close binary stars like Eclipsing Binaries, RS Canum Venaticorum, and Ellipsoidal variables also show emission linked to accretion disks; delta Scuti, gamma Doradus, SX Phoenicis, and Beta Cephei variables have emission lines related to radial pulsations. Although Long Period Variables and Young Stellar Objects can have emission, in our study we found it to be rather weak. For Cepheid variables, emission lines are not expected. However, one possible origin for Anoma-

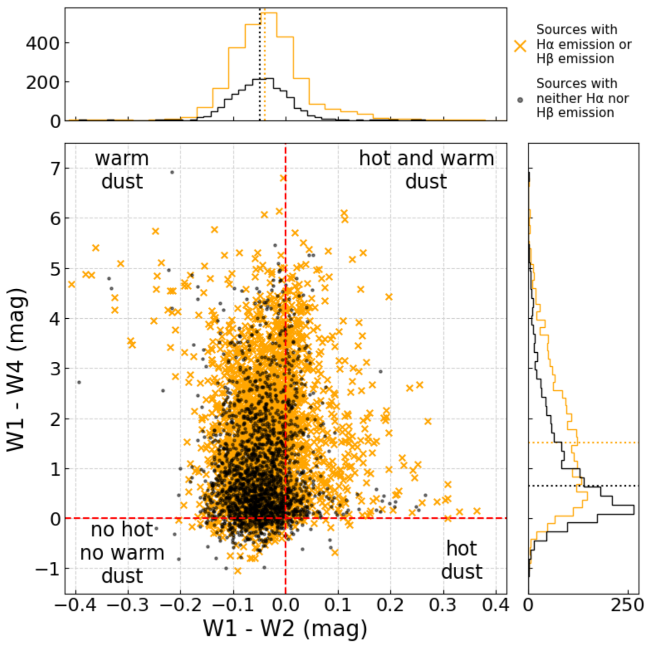

FIG. 5: Color-Color Diagram constructed using *WISE* photometry. Histograms show the distribution of IR excess in hotter and colder *WISE* bands for emitters and non-emitters. Dotted lines on histograms represent the median value.

lous Cepheids is believed to be mass transfer in a stellar binary system, which would again explain the emission due to the accretion mechanism.

From our analysis, we see that variability and emission can be connected along with accretion processes in some cases and, thus, to IR excess. However, it is not exclusive to any particular type of variable star. Thus, variability should be studied further using the light curves of the stars to distinguish possible LRN precursors from stars with well-understood variability processes.

The accretion processes in the disks of single stars and close binaries undergoing mass transfer can cause radiation that excites/ionizes hydrogen, which recombines creating emission lines. These disks, which contain hot/warm dust, are linked to IR excess, observed in both CMDs and CCDs (Bonanos et al. [5]). In Figure 5, stars with mid-IR colors near 0, i.e. no IR excess, are stars with no dusty disks, while stars with increasing values of W1-W4 have mid-IR excess linked to warm dust, and positive values of the W1-W2 color indicate hotter disks. While both distributions of stars with and without emission present IR excess, stars with emission have higher W1-W4 values and non-emitting stars are more clumped up, showing no IR excess. This shows that stars with emission in our HG sample had larger mid-IR excess. The presence of both emission and mid-IR excess in stars from our sample hints at the existence of close binaries undergoing mass transfer, therefore, possible LRN precursors. High-resolution spectroscopy is needed to establish their nature.

Our final analysis focused on exploring the light curves of stars satisfying all four criteria: being in the HG, being identified as variables, showing Hα/Hβ emission, and displaying mid-IR excess. Unfortunately, from a set of 193 stars with such conditions, only 88 were contained in ZTF. Out of these, 56 were not known variables in *SIMBAD*. Although detailed light curve analysis is out of the scope of this work, we detect sources with periodic variations, such as eclipses or pulsations (e.g. Figures 8a, 8d, 8f, 8k, 8l...), and also sources with non-periodic variability, similar to small outbursts (Figures 8h, 8m, 8s, 8z). These sources deserve further study, as they likely are new mass-transferring binary systems or single stars with enhanced activity.

V. CONCLUSIONS

Following the steps of previous investigations on Luminous Red Novae and their possible progenitors, in this work we conducted a study of Galactic stars in the Hertzsprung gap. We investigated their variability, emission, and their mid-infrared excess. We found that the presence of variability, Hα and Hβ emission, and mid-infrared excess was not always related and may appear in many stars in the Hertzsprung gap. Nevertheless, close binary stars crossing the Hertzprung gap—and so possibly LRN precursors—show a particular, long-term variability that can distinguish them from other variable stars. They also have dusty disks, detectable via infrared excess, and show emission in the main Balmer lines, which is likely caused by accretion from the disk. We selected a sample of sources satisfying these criteria and investigated the available lightcurves which allowed us to identify new variable stars. Further work will focus on the close examination of the variability type, emission, and infrared excess. Along with high-resolution spectra, it will provide a characterization of the precise nature of these sources and further confirm or reject them as LRN precursors.

Acknowledgments

I would like to thank my advisor Nadejda Blagorodnova for guiding me through the project, providing me with all the time and assistance I needed, and giving me the chance of getting closer to astrophysical research. I would also like to thank Francesca Figueras for introducing me to Nadejda, and to Carme Jordi, Friedrich Anders, and Michael Weiler for fruitful discussions.

[1] Addison, H., et al. 2022, MNRAS, 517, 1884
[2] Anders, F., et al. 2022, A&A, 658, A91
[3] Bellm, E. C., et al. 2019, PASP, 131, 018002
[4] Blagorodnova, N., et al. 2017, Astrophys. J. , 834, 107
[5] Bonanos, A. Z., et al. 2010, AJ, 140, 416
[6] Cutri, R. M., et al. 2021, VizieR Online Data Catalog, II/328
[7] Gaia Collaboration, et al. 2016, A&A, 595, A1
[8] Gray, R. O. & Corbally, Christopher, J. 2009, Stellar Spectral Classification
[9] Montegriffo, P., et al. 2022, arXiv e-prints, arXiv:2206.06205
[10] Paczynski, B. 1976, in Structure and Evolution of Close Binary Systems, ed. P. Eggleton, S. Mitton, & J. Whelan, Vol. 73, 75
[11] Paxton, B. 2021, Modules for Experiments in Stellar Astrophysics (MESA), Zenodo
[12] Piascik, A. S., et al. 2014, in Society of Photo-Optical Instrumentation Engineers (SPIE) Conference Series, Vol. 9147, Ground-based and Airborne Instrumentation for Astronomy V, ed. S. K. Ramsay, I. S. McLean, & H. Takami, 91478H
[13] Ruz-Mieres, D. 2022, gaia-dpci/GaiaXPy: GaiaXPy 1.2.0, Zenodo
[14] Tylenda, R., et al. 2011, A&A, 528, A114
[15] Weiler, M., et al. 2023, A&A, 671, A52
[16] Wenger, M., et al. 2000, A&AS, 143, 9

VI. APPENDIX

A. Flags used in catalogs

In this section a summarized explanation of the flags used to curate the data extracted from the *ALLWISE* catalog can be found. The full explanation of the used flags and more can be found in the following *WISE* webpage: https://wise2.ipac.caltech.edu/docs/release/allwise/expsup/sec2_1a.html.

- `cc_flags`: Contamination and confusion flags. One character for each of the four bands indicating photometry and/or position measurements of a source may be contaminated or biased due to proximity to an image artifact. Can take the subsequent values:
  - **D**,**d** - Diffraction spike.
  - **P**,**p** - Persistence.
  - **H**,**h** - Halo.
  - **O**,**o** - Optical ghost.
  - **0** (number zero) - Source is unaffected by known artifacts.

  Lower-case letters correspond to a detection believed to be real but measurements may be contaminated. Upper-case letters correspond to a spurious detection of an artifact.

- `ext_flag`: Extended source flag. The values of the `ext_flag` indicate the following conditions:
  - **0** - The source shape is consistent with a point-source and the source is not associated with or superimposed on a 2MASS XSC source.
  - **1** - The profile-fit photometry goodness-of-fit, $w?rchi2$, is > 3.0 in one or more bands.
  - **2** - The source falls within the extrapolated isophotal footprint of a 2MASS XSC source.
  - **3** - The profile-fit photometry goodness-of-fit, $w?rchi2$, is > 3.0 in one or more bands, and The source falls within the extrapolated isophotal footprint of a 2MASS XSC source.
  - **4** - The source position falls within 5" of a 2MASS XSC source.
  - **5** - The profile-fit photometry goodness-of-fit, $w?rchi2$, is > 3.0 in one or more bands, and the source position falls within 5" of a 2MASS XSC source.

- `ph_qual`: Photometric quality flag. One character for each of the four bands, that provides a summary of the quality of the profile-fit photometry.
  - **A** - Source is detected in this band with a flux signal-to-noise ratio $w?snr > 10$.
  - **B** - Source is detected in this band with a flux signal-to-noise ratio $3 < w?snr < 10$.
  - **C** - Source is detected in this band with a flux signal-to-noise ratio $2 < w?snr < 3$.
  - **U** - Upper limit on magnitude. Source measurement has $w?snr < 2$. The profile-fit magnitude $w?mpro$ is a 95% confidence upper limit.
  - **X** - A profile-fit measurement was not possible at this location in this band. The value of $w?mpro$ and $w?sigmpro$ will be "null" in this band.
  - **Z** - A profile-fit source flux measurement was made at this location, but the flux uncertainty could not be measured. The value of $w?sigmpro$ will be "null" in this band. The value of $w?mpro$ will be "null" if the measured flux, $w?flux$, is negative, but will not be "null" if the flux is positive. If a non-null magnitude is present, it corresponds to the true flux, and not the 95% confidence upper limit. This occurs for a small number of sources found in a narrow range of ecliptic longitude which were covered by a large number of saturated pixels from 3-Band Cryo single-exposures.

The values we used for these flags were: `cc_flags` = 0000; `ext_flag` = 0, and `ph_qual` = A, B or C.

B. Variable stars classification and spectrums

TABLE I: Table containing the classifier name and description found in the *Gaia Archive* for variable stars in the DR3. The number of sources and emitter for each type found in our sample is shown.

Classifier Name	Classifier Description	# of sources	# of emitters
RR	RR Lyrae stars of the following types: fundamental-mode, first-overtone, double mode, and anomalous double mode.	4516	1016 (22%)
ECL	Eclipsing Binaries of types: Beta Persei (Algol), Beta Lyrae, and W Ursae Majoris.	4004	312 (7.8%)
RS	RS Canum Venaticorum type variable.	2095	416 (20%)
DSCT|GDOR|SXPHE	Set of variable types: delta Scuti, gamma Doradus, and SX Phoenicis.	1835	37 (2.0%)
CEP	Cepheid variable types: delta Cepheid, anomalous Cepheid, and type-II Cepheid.	1537	226 (15%)
LPV	Long Period Variable stars of types: omicron Ceti (Mira), OGLE Small Amplitude Red Giants, and semiregular.	526	218 (41%)
YSO	Young Stellar Object.	352	64 (18%)
BE|GCAS|SDOR|WR	Subset of eruptive variable types: B-type emission line star, Gamma Cassiopeiae, S Doradus, and Wolf-Rayet.	265	85 (32%)
BCEP	Beta Cephei type variable.	214	5 (2.3%)
ACYG	Alpha Cygni-type variable.	142	41 (29%)
ELL	Ellipsoidal variable.	93	32 (34%)
ACV|CP|MCP|ROAM|ROAP|SXARI	Set of variable types: alpha2 Canum Venaticorum, (Magnetic) Chemical Peculiar star, Rapidly Oscillating Am/Ap star, and SX Arietis variable.	32	1 (3.1%)

FIG. 6: Close up around the Hβ (left) and the Hα (right) lines of the average (scaled) spectrum for each variable type in our sample which presented hydrogen emission. All the stars in one type (solid green line), stars showing $H\alpha$ emission (dashed red line), and stars showing $H\beta$ emission (dotted blue line). One σ of error for each of the lines respectively is presented.

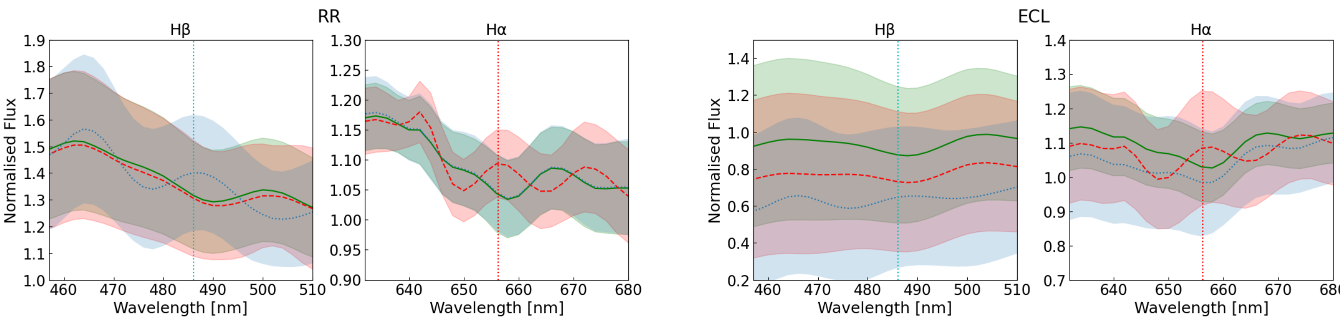

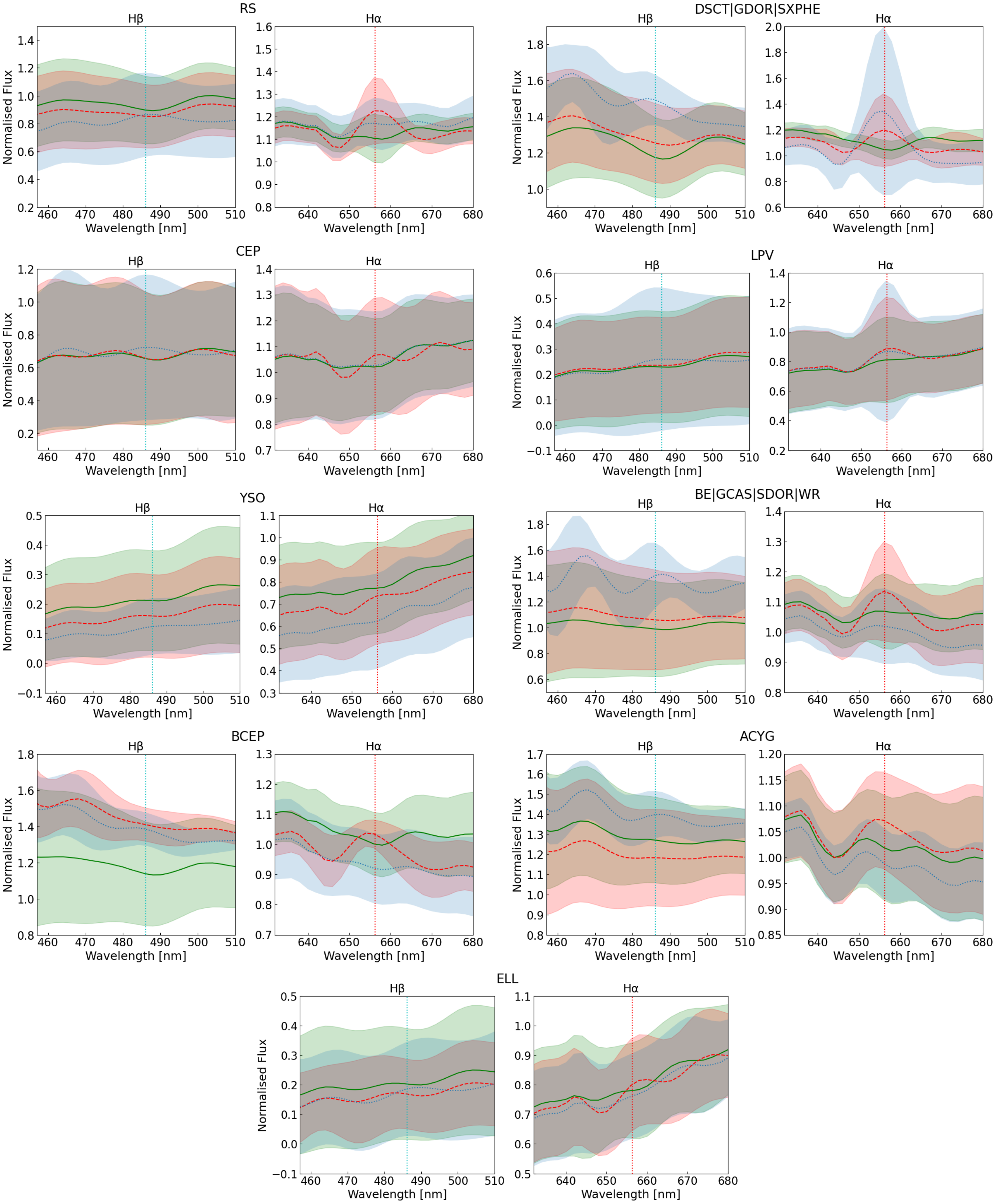
RS
DSCT|GDOR|SXPHE
CEP
LPV
YSO
BE|GCAS|SDOR|WR
BCEP
ACYG
ELL
Hβ
Hα
Normalised Flux
Wavelength [nm]

C. ZTF light curves

FIG. 8: *ZTF* light curves for 56 sources that we found with variability, hydrogen emission, and mid-IR excess. We believe that some of them have a high probability of being LRN precursors and should be further investigated. 23 of them had a classification in *SIMBAD* which is shown as a title.

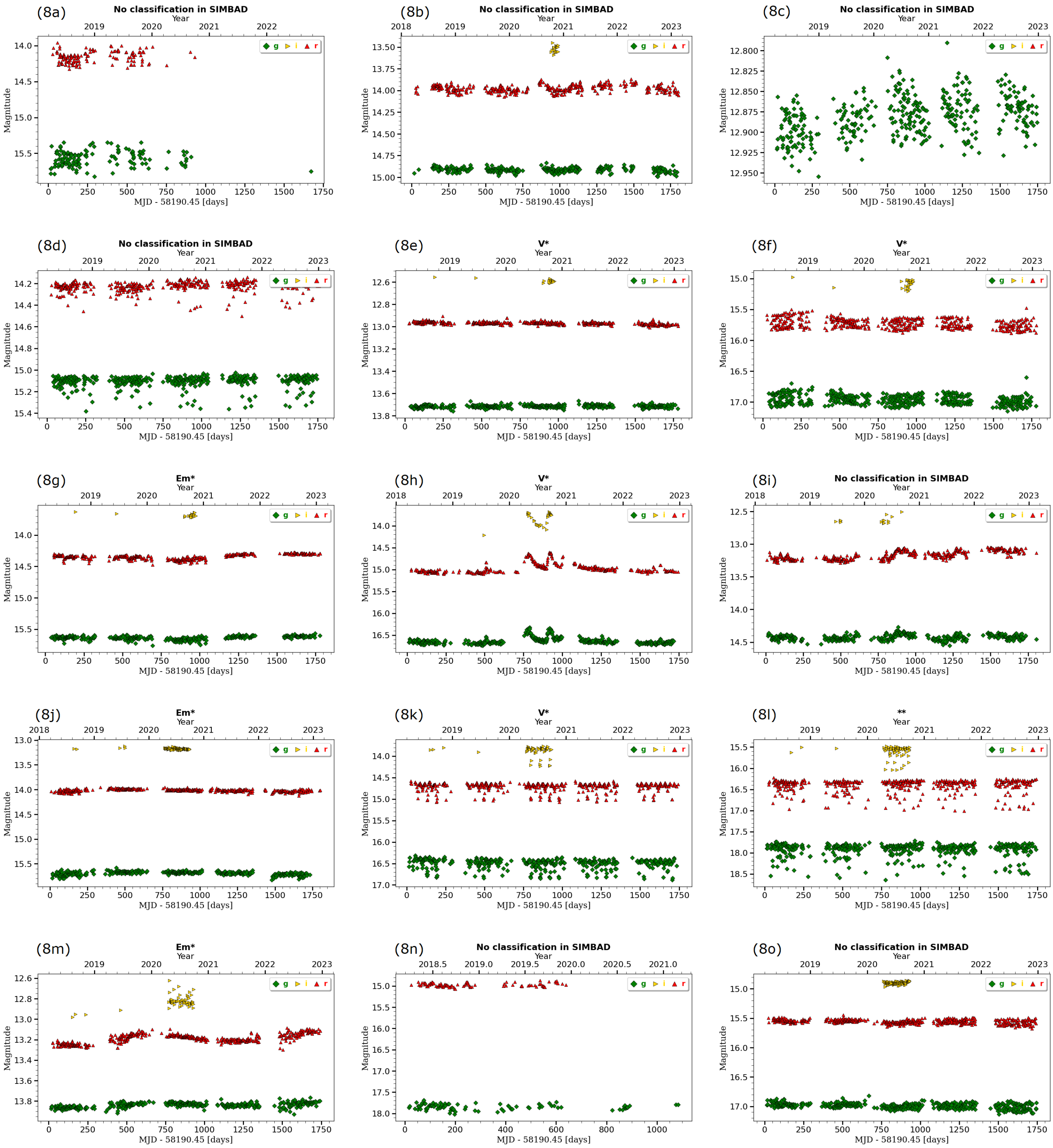

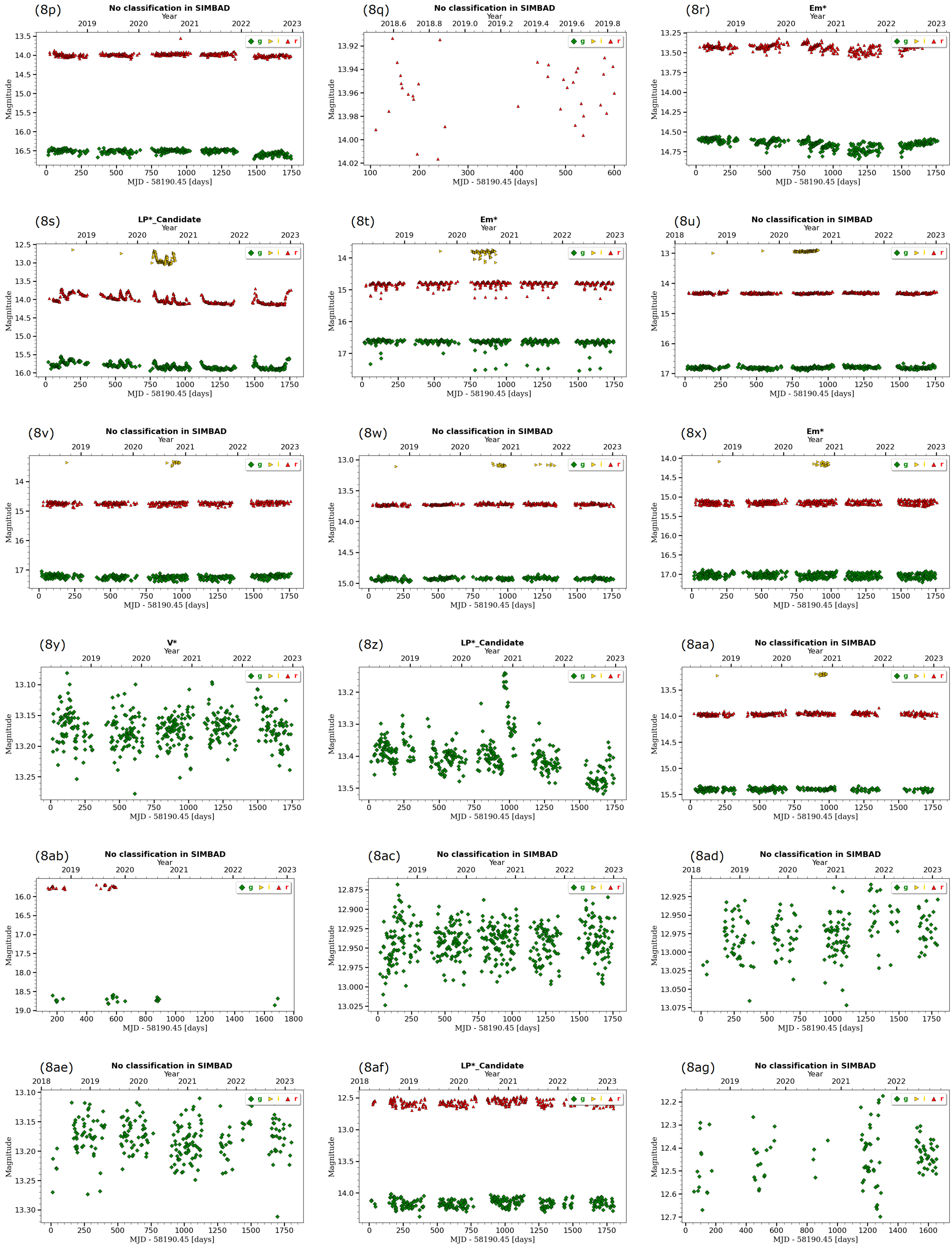
(8p)
No classification in SIMBAD
(8q)
No classification in SIMBAD
(8r)
Em*
(8s)
LP*_Candidate
(8t)
Em*
(8u)
No classification in SIMBAD
(8v)
No classification in SIMBAD
(8w)
No classification in SIMBAD
(8x)
Em*
(8y)
V*
(8z)
LP*_Candidate
(8aa)
No classification in SIMBAD
(8ab)
No classification in SIMBAD
(8ac)
No classification in SIMBAD
(8ad)
No classification in SIMBAD
(8ae)
No classification in SIMBAD
(8af)
LP*_Candidate
(8ag)
No classification in SIMBAD
Year
Magnitude
MJD - 58190.45 [days]
g
i
r

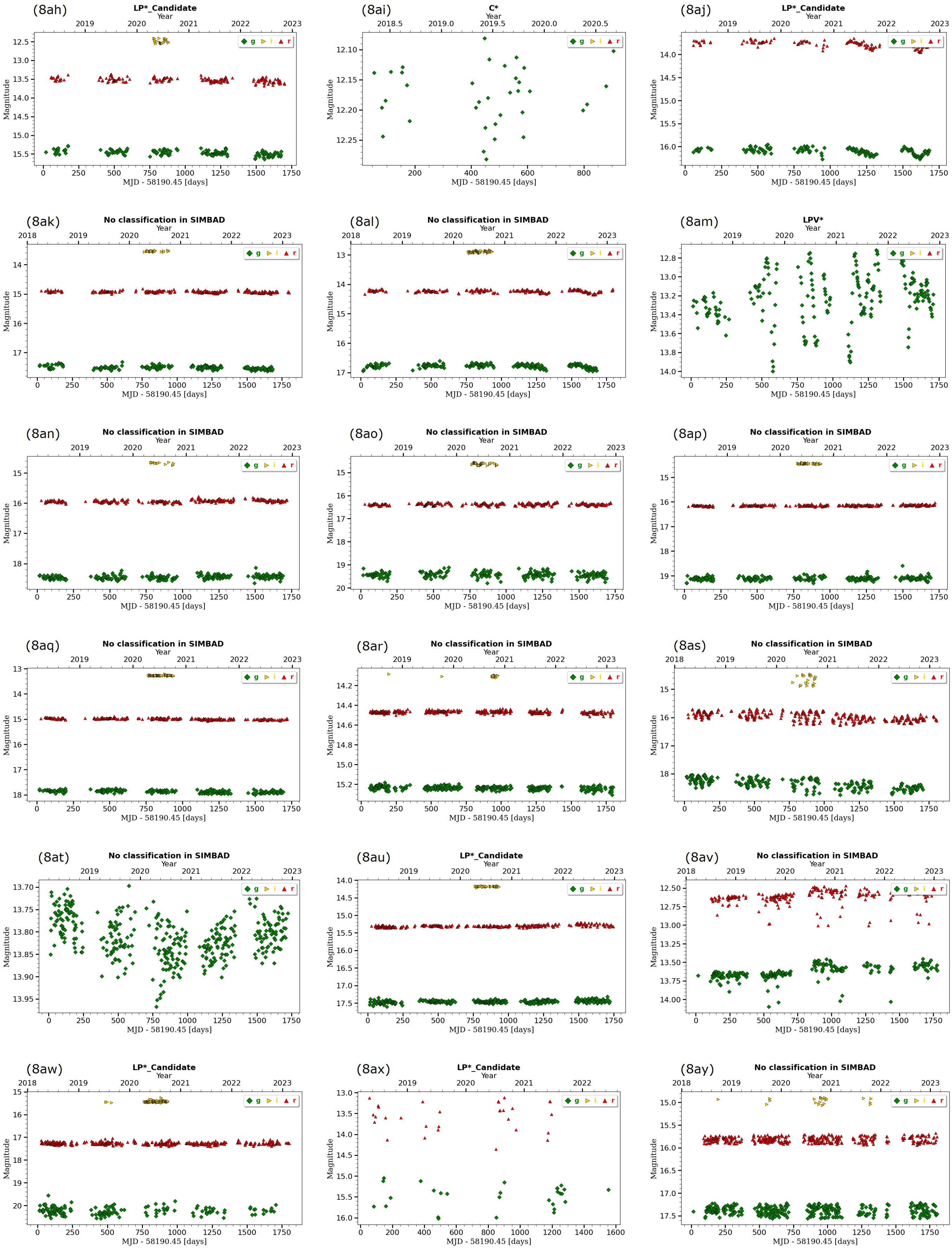
(8ah) LP*_Candidate
(8ai) C*
(8aj) LP*_Candidate
(8ak) No classification in SIMBAD
(8al) No classification in SIMBAD
(8am) LPV*
(8an) No classification in SIMBAD
(8ao) No classification in SIMBAD
(8ap) No classification in SIMBAD
(8aq) No classification in SIMBAD
(8ar) No classification in SIMBAD
(8as) No classification in SIMBAD
(8at) No classification in SIMBAD
(8au) LP*_Candidate
(8av) No classification in SIMBAD
(8aw) LP*_Candidate
(8ax) LP*_Candidate
(8ay) No classification in SIMBAD
Year
Magnitude
MJD - 58190.45 [days]
g
i
r

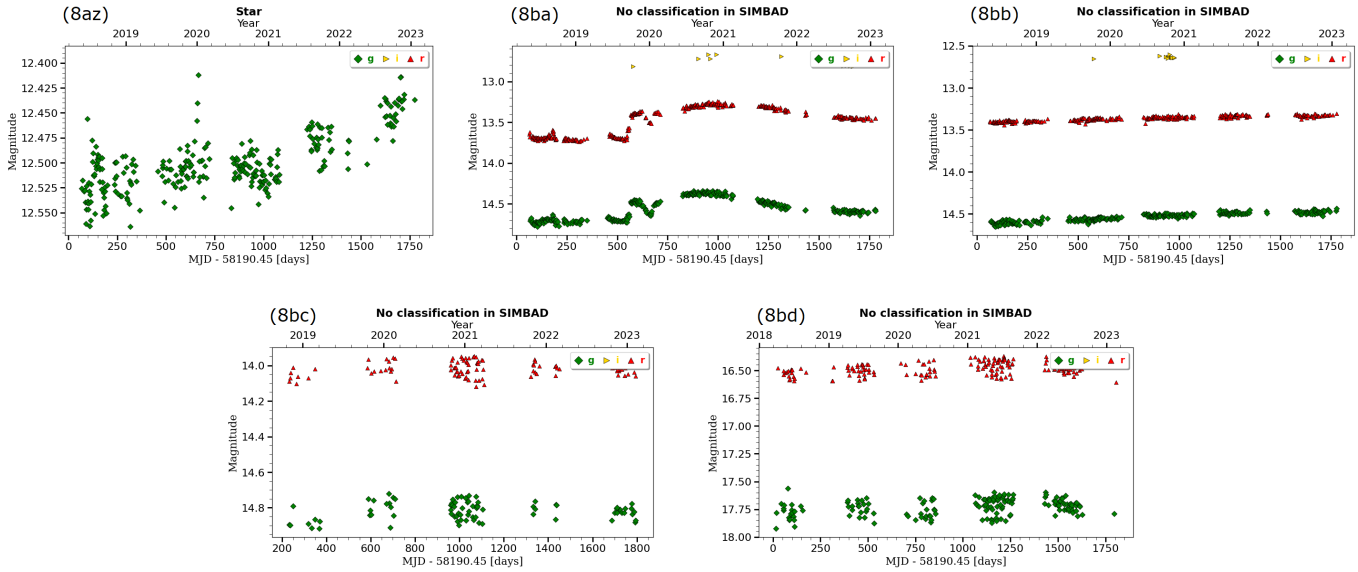
(8az)
Star
(8ba)
No classification in SIMBAD
(8bb)
No classification in SIMBAD
(8bc)
No classification in SIMBAD
(8bd)
No classification in SIMBAD
Year
Magnitude
MJD - 58190.45 [days]
g
i
r